

Individual differences and time-varying features of modular brain architecture



Xuhong Liao^{a,b,c}, Miao Cao^{a,b,c}, Mingrui Xia^{a,b,c}, Yong He^{a,b,c,*}

^a National Key Laboratory of Cognitive Neuroscience and Learning, Beijing Normal University, Beijing 100875, China

^b IDG/McGovern Institute for Brain Research, Beijing Normal University, Beijing 100875, China

^c Beijing Key Laboratory of Brain Imaging and Connectomics, Beijing Normal University, Beijing 100875, China

ARTICLE INFO

Keywords:

Connectomics
Association cortex
Dynamics
Graph theory
Modularity
Connector

ABSTRACT

Recent studies have suggested that human brain functional networks are topologically organized into functionally specialized but inter-connected modules to facilitate efficient information processing and highly flexible cognitive function. However, these studies have mainly focused on group-level network modularity analyses using “static” functional connectivity approaches. How these extraordinary modular brain structures vary across individuals and spontaneously reconfigure over time remain largely unknown. Here, we employed multiband resting-state functional MRI data (N=105) from the Human Connectome Project and a graph-based modularity analysis to systematically investigate individual variability and dynamic properties in modular brain networks. We showed that the modular structures of brain networks dramatically vary across individuals, with higher modular variability primarily in the association cortex (e.g., fronto-parietal and attention systems) and lower variability in the primary systems. Moreover, brain regions spontaneously changed their module affiliations on a temporal scale of seconds, which cannot be simply attributable to head motion and sampling error. Interestingly, the spatial pattern of intra-subject dynamic modular variability largely overlapped with that of inter-subject modular variability, both of which were highly reproducible across repeated scanning sessions. Finally, the regions with remarkable individual/temporal modular variability were closely associated with network connectors and the number of cognitive components, suggesting a potential contribution to information integration and flexible cognitive function. Collectively, our findings highlight individual modular variability and the notable dynamic characteristics in large-scale brain networks, which enhance our understanding of the neural substrates underlying individual differences in a variety of cognition and behaviors.

Introduction

Modularity (i.e., the decomposability of a system into small modules) is a ubiquitous organization principle in most complex systems, including social, economic and biological networks (Hartwell et al., 1999). Using human resting-state functional MRI (R-fMRI) that can capture the brain's intrinsic or spontaneous activity (Biswal et al., 1995), recent studies have demonstrated that the human brain functional network during rest is organized into several functionally specialized but interconnected modules, such as the sensorimotor, visual, default-mode, fronto-parietal and attention modules (He et al., 2009; Meunier et al., 2009; Power et al., 2011). This intrinsically cohesive modular structure, which is presumably shaped by evolutionary constraints, allows the brain to enable efficient information communication with low wiring costs (Bullmore and

Sporns, 2012) and fast adaption to changeable task demands (Bassett et al., 2011; Braun et al., 2015; Liang et al., 2016), and serves as a fundamental network basis for cognitive flexibility (Bertolero et al., 2015). Recent studies found that these brain modules exhibit distinct cerebral blood flow rates (Liang et al., 2013) and are closely associated with the correlated gene expression (Richiardi et al., 2015), further suggesting underlying physiological and molecular mechanisms. Notably, two important questions remain to be further elucidated, despite greatly growing interests in investigating the intrinsic network modules in the resting human brain.

The first question concerns individual differences in the functional modular brain architecture during rest. Human brain structure and function greatly vary across individuals. For example, structural brain imaging and histology studies show remarkable structural variability in language areas in either the regional cytoarchitecture (Amunts et al.,

* Corresponding author at: National Key Laboratory of Cognitive Neuroscience and Learning, IDG/McGovern Institute for Brain Research, Beijing Key Laboratory of Brain Imaging and Connectomics, Beijing 100875, China.

E-mail address: yong.he@bnu.edu.cn (Y. He).

<http://dx.doi.org/10.1016/j.neuroimage.2017.02.066>

Received 28 January 2017; Accepted 23 February 2017

Available online 24 February 2017

1053-8119/ © 2017 Elsevier Inc. All rights reserved.

1999; Amunts et al., 2004; Eickhoff et al., 2005) or cortical morphology (Hill et al., 2010a). Functional brain imaging studies based on task- and R-fMRI reveal substantial functional variability in the association cortex (e.g., lateral frontal areas) in either task-evoked activations (Frost and Goebel, 2012; Pinel et al., 2007), intrinsic functional connectivity (Finn et al., 2015; Mueller et al., 2013), cortical parcellations (Langs et al., 2016; Wang et al., 2015a) or functional systems (Gordon et al., 2015). These structural and functional variations may origin from the joint effects of genetic and environmental factors (Brun et al., 2009; Chen et al., 2012; Gao et al., 2014; Hill et al., 2010b; Johnson et al., 2009; Petanjek et al., 2011) and have greatly advanced our understanding of the neural substrates of individual differences in cognition and behavior. Quantifying the inter-subject variability in the intrinsic modular organization would provide system-level insights. Until recently, only two R-fMRI studies directly examined individual differences in the functional modular architecture, with a primary focus on the consistent network modules across individuals (Moussa et al., 2012) or the deviation of individual modular structures from the group-level organization (Laumann et al., 2015). However, how the intrinsic modular brain architecture, especially the constitution of functional modules, varies across individuals remains largely unknown.

The second question concerns the time-varying dynamics of modular architecture in the brain functional networks. Recent task-related fMRI studies demonstrated that the dynamic reconfiguration of the functional modular structure in response to task demands are associated with individual performances in motor skill learning (Bassett et al., 2011) and working memory tasks (Braun et al., 2015). Existing literature has suggested that both the dynamic functional architecture during tasks and the individual behavioral performances can be shaped by the intrinsic brain networks during rest (Cole et al., 2014; Sadaghiani et al., 2015; Schultz and Cole, 2016; Wang et al., 2016). Hence, exploring the time-varying characteristics of intrinsic modular organization may provide fundamental insights into flexible cognitive functions (Anderson, 2014; Pessoa, 2014). Several R-fMRI studies demonstrated that during the resting state, the functional modular architecture, such as network modularity and the connectivity strength associated with the modules, temporally changes on a short time scale (e.g., seconds) (Allen et al., 2014; Betzel et al., 2016; Di and Biswal, 2015; Jones et al., 2012; Schaefer et al., 2014). However, how the brain regions dynamically switch their module affiliations over time and the functional implications remain to be elucidated.

To address these issues, in the present study we employed multiband R-fMRI data and a graph-based modularity analysis to systematically explore the individual variability and the time-varying characteristics of the intrinsic modular architectures in the human brain. Specifically, for each subject, we constructed large-scale static and sliding window-based dynamic functional networks and tracked the modular architectures across subjects or time. Given that higher-order cognitive functions primarily involving association areas (e.g., frontoparietal areas) (Yeo et al., 2015) exhibit remarkable individual differences, we hypothesized that the association regions would show large inter- and/or intra-subject modular variability. We further investigated whether the subject-specific functional modular architecture and the temporal characteristics were reproducible across repeated scanning sessions. Finally, we examined the associations between inter-/intra-subject modular variability and the functional connectors and cognitive flexibility (Yeo et al., 2015).

Materials and methods

Subjects and data acquisition

Multiband resting-state fMRI (R-fMRI) data were acquired from the publicly available Q2 Data Release of the Human Connectome

Project (HCP) (Van Essen et al., 2013). The data set included 142 healthy subjects, of which 132 subjects underwent repeated R-fMRI scanning in two sessions (Table S1). Written informed content was obtained from each subject, and the scanning protocol was approved by the Institutional Review Board of Washington University in St. Louis, MO, USA (IRB #20120436).

All subjects underwent multimodal imaging scans in a customized 32-channel Siemens 3T “Connectome Skyra” scanner at Washington University. For each subject, four R-fMRI runs were collected in two sessions, with two runs separately acquired per session through phase encoding in the left-to-right and right-to-left directions. Specifically, each R-fMRI run was acquired using a multiband gradient-echo-planar imaging sequence as follows: time repetition=720 ms; time echo=33.1 ms; flip angle=52°; field of view=208×180 mm²; matrix=104×90; 72 slices; voxel size=2×2×2 mm³; multiband factor=8 and 1200 volumes (i.e., 14.4 min). During the scanning, the subjects maintained a relaxed fixation on a cross. Notably, the R-fMRI data from 27 subjects were excluded from the analysis due to missing time points (N=3) or excessive head motion (N=24) (see “Data preprocessing”) (Table S1). The data from the remaining 105 subjects (age 22–35 years, 37 males) were used for the final analysis. In the present study, the R-fMRI data from the first session (i.e., S1) were used for the main analysis and the data from the second session (i.e., S2) were used for the validation and reproducibility analysis unless otherwise indicated. To reduce the potential influence of different phase encoding directions, only the left-to-right encoded runs are included here.

Data preprocessing

We obtained minimally preprocessed R-fMRI data conducted using HCP Functional Pipeline v2.0 (Glasser et al., 2013) involving gradient distortion correction, head motion correction, image distortion correction and spatial transformation to the Montreal Neurological Institute space using one step spline resampling from the original functional images followed by then intensity normalization. Notably, functional data from 24 subjects were discarded due to their large head motions in either run with criteria of a translation/rotation > 3 mm/° or a mean framewise head motion > 0.14 mm (Finn et al., 2015). The framewise head motion parameters were extracted from ‘relativeRMS_mean.txt’ in the Q2 release. In this study, these minimally preprocessed images were further analyzed using SPM8 (<http://www.fil.ion.ucl.ac.uk/spm>) and DPARSF (Yan and Zang, 2010). Briefly, first the linear trend was removed from these functional images. Then, several nuisance signals were regressed from the time course of each voxel using multiple linear regression, including twenty-four head motion parameters (Friston et al., 1996), cerebrospinal fluid, white matter and global brain signals (Birn et al., 2006; Fox et al., 2009). Finally, temporal band-pass filtering (0.01–0.1 Hz) was performed to reduce the influence of low-frequency drifts and the high-frequency physiological noises (Biswal et al., 1995; Lowe et al., 1998). The resulting time courses were used for the brain network construction and analysis.

Construction of functional brain networks

The brain network construction was implemented with GRETNA (<http://www.nitrc.org/projects/gretna/>) (Wang et al., 2015b). In this study, we constructed the whole-brain functional networks at the macroscopic level, in which nodes represented regions of interest (ROIs) and edges represented inter-regional functional connectivity. Specifically, we employed a functionally defined atlas (Power et al., 2011) to generate 264 nodal ROIs, each of which denoted 5-mm radius spheres centered on previously reported coordinates. This atlas ensures the functional significance of the brain network nodes and simultaneously reduces the chance of signal blurring from multiple

functional areas within a node (Wig et al., 2011). It has been widely used in both resting- and task-state brain network studies (Cole et al., 2014; Cole et al., 2013; Gu et al., 2015; Power et al., 2013; Sadaghiani et al., 2015; Schultz and Cole, 2016). Using the preprocessed R-fMRI data, we obtained the time course of each nodal ROI by averaging the time courses of all voxels within the ROI, which was used for the subsequent construction of the static and dynamic brain networks. We also validated our main findings using two other parcellation schemes (see “Validation analysis”).

Static brain network construction

For each subject, first we computed Pearson's correlation coefficients between each pair of nodes using the whole-run time courses and generated a 264×264 symmetric correlation matrix. Then, a static weighted functional network was constructed by thresholding the correlation matrix with a given connectivity density S and the correlation values for the preserved edges were retained as edge strengths. Here, the connectivity density was selected as $S=15\%$, which maintained the high connectedness of the brain networks and simultaneously removed as many spurious correlations as possible. We also assessed the effects of different connectivity densities on the main results (see “Validation analysis”). A group-level static weighted functional network was also constructed as a reference by thresholding a mean correlation matrix with the same network density ($S=15\%$). The mean correlation matrix was generated by averaging individual Fisher's r -to- z transformed correlation matrices across subjects, followed by an inverted Fisher's transformation. Notably, all negative correlations were excluded from the networks due to their ambiguous physiological interpretations (Fox et al., 2009; Murphy et al., 2009; Weissenbacher et al., 2009; Yan et al., 2013).

Dynamic brain network construction

For each subject, we employed a widely-used sliding window approach to estimate dynamic functional connectivities across time (Calhoun et al., 2014; Hutchison et al., 2013a). Briefly, we computed Pearson's correlation coefficients among each pair of nodes using the time course segments within a time window. The window length was set as 139 TRs (i.e., 100 s), which allowed us to estimate the functional connectivity over the low-frequency band of interest (0.01–0.1 Hz) with adequate time points (at least one period) and simultaneously capture the time-varying characteristics of the functional connectivity (Betzel et al., 2016; Leonardi and Van De Ville 2015; Liao et al., 2015). By shifting the time window forward with a step of one TR (i.e., 720 ms), for each subject we obtained 1062 264×264 symmetric correlation matrices. Then, we thresholded each windowed correlation matrix with a fixed connectivity density ($S=15\%$) to generate dynamic weighted functional networks for each subject. We also assessed the effects of different sliding window lengths and various network densities on the main results (see “Validation analysis”).

Detection of functional brain modules

Modules (also known as communities) generally correspond to groups of densely connected nodes with sparse between-group connections (Newman, 2004). Given modular partition p of a network, the modularity $Q(p)$ of the network is calculated as (Newman, 2004)

$$Q(p) = \sum_{s=1}^{N_M} \left[\frac{l_s}{m} - \left(\frac{d_s}{2m} \right)^2 \right], \quad (1)$$

where N_M is the number of modules, m denotes the total edge strength in the network, l_s indicates the total edge strength within module s , and d_s is the total degree value of the nodes in module s . The nodal degree indicates the total strength of the edges directly attached to the node.

In practice, a network shows a strong modular structure if the modularity index $Q(p)$ is larger than 0.3 (Newman, 2004). In human brain networks, the functional module is usually referred to as a densely connected group of brain regions. Here, we employed the Infomap algorithm for functional module detection (Rosvall and Bergstrom, 2008) because this algorithm captures the information propagating flow in the network and has been used to reveal brain modules in good agreement with task-related functional systems (Power et al., 2011) or cognitive components (Bertolero et al., 2015). For each subject, we identified the modular architecture by applying the Infomap algorithm to the static and dynamic weighted functional networks. For a given modular partition p in a static or a windowed dynamic brain network, the modularity index $Q(p)$ and the number of modules N_M were calculated. Of note, when counting the number of modules, small modules with less than five nodes (e.g., isolated nodes) were ignored. We also validated our main results using other module detection algorithms (see “Validation analysis”).

Tracking modular architectures across and within subjects

To date, functional modules of human brain networks are often identified at a population level from a static perspective (e.g., He et al., 2009; Meunier et al., 2009; Power et al., 2011; Power et al., 2013). In the current study, we examined the functional modular structures from two rarely studied aspects: inter-subject variability in static brain modules and intra-subject temporal variability in dynamic brain modules. We proposed the following procedure to compare the pairwise topological differences in modular structures which were extracted from different individuals or different time windows within one individual.

Comparison of modular structures

Given two modular structures or partitions i and j obtained from two individuals or two time windows, their topological differences can be quantitatively assessed at both the overall and nodal levels.

- i) Overall Level. The overall similarity between two modular structures can be measured based on their module assignment labels using adjusted mutual information (AMI, Vinh et al., 2010). The AMI index is often applied to evaluate how well two modular partitions match, with the correction of the agreement by chance. Specifically, the AMI for two partitions i and j is calculated as (Vinh et al., 2010)

$$AMI(i, j) = \frac{MI(i, j) - E\{MI(i, j)\}}{\max\{H(i), H(j)\} - E\{MI(i, j)\}} \quad (2)$$

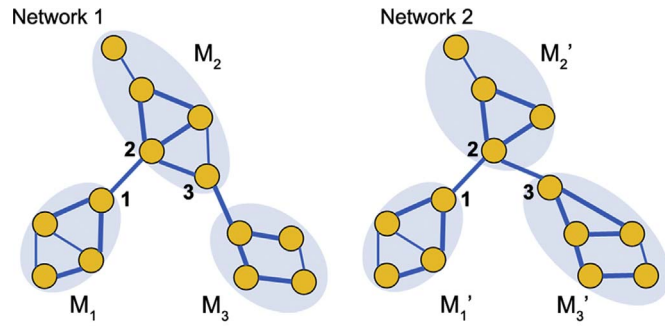
where $MI(i, j)$ indicates the mutual information between two partitions, $E\{MI(i, j)\}$ denotes the expected mutual information between two random partitions, and $H(i)$ denotes the entropy of the partition i . The estimation of AMI is independent on the absolute values of the module labels. It ranges from 0 to 1, with 0 indicating two completely different partitions and 1 indicating two identical partitions.

Given a partition i , its entropy $H(i)$ is defined as

$$H(i) = - \sum_{m=1}^M P_i(m) \log P_i(m) \quad (3)$$

where $P_i(m)$ indicates the probability of nodes locating in module m in partition i . The mutual information $MI(i, j)$ measures the mutual dependence between two partitions i and j , and is defined as

$$MI(i, j) = \sum_{m=1}^M \sum_{n=1}^N P(m, n) \log \frac{P(m, n)}{P_i(m)P_j(n)} \quad (4)$$



$$MV_1(1,2) = 1 - \frac{|M_1 \cap M_1'|}{|M_1|} \cdot \frac{|M_1 \cap M_1'|}{|M_1'|} = 1 - \frac{4}{4} \cdot \frac{4}{4} = 0$$

$$MV_2(1,2) = 1 - \frac{|M_2 \cap M_2'|}{|M_2|} \cdot \frac{|M_2 \cap M_2'|}{|M_2'|} = 1 - \frac{4}{5} \cdot \frac{4}{5} = \frac{1}{5}$$

$$MV_3(1,2) = 1 - \frac{|M_2 \cap M_3'|}{|M_2|} \cdot \frac{|M_2 \cap M_3'|}{|M_3'|} = 1 - \frac{1}{5} \cdot \frac{1}{5} = \frac{24}{25}$$

Fig. 1. Schematic of the estimation of nodal modular variability (MV) across two networks. Network 1 includes three modules (M_1 , M_2 and M_3) and Network 2 includes three modules (M_1' , M_2' and M_3'). For each node, first we identified the functional modules to which this node separately belonged in two networks. Then, the modular variability was calculated by subtracting the extent of the overlap between these two modules from 1. For example, node 1 belongs to module M_1 in Network 1 and M_1' in Network 2, respectively. Because modules M_1 and M_1' completely overlap, the modular variability of node 1 equals zero. The modular variability of the other nodes can be estimated in similar ways, where node 2 exhibits small modular variability and node 3 exhibits large modular variability.

where $P(m, n)$ indicates the probability of nodes belonging to both module m in partition i and module n in partition j .

- ii) Nodal Level. For each node, we can evaluate its module affiliation variability between two modular partitions through a metric of modular variability (MV) (Fig. 1). For example, for a given node k between two modular partitions i and j obtained from two individuals or two time windows, we can calculate $MV_k(i, j)$ (Steen et al., 2011) as

$$MV_k(i, j) = 1 - \frac{|X_k(i) \cap X_k(j)|}{|X_k(i)|} \cdot \frac{|X_k(i) \cap X_k(j)|}{|X_k(j)|}, \quad (5)$$

where $X_k(i)$ and $X_k(j)$ denote the module labels to which node k belongs in modular partitions i and j , respectively. $X_k(i) \cap X_k(j)$ represents the common node set between modules $X_k(i)$ and $X_k(j)$, and $|X_k(i) \cap X_k(j)|$ denotes the number of nodes in the common node set. For node k between modular structures i and j , a small overlap between the two modules $X_k(i)$ and $X_k(j)$ indicates large module affiliation variability.

Likewise, given a set of n ($n > 2$) modular partitions (i.e., the number of subjects or time windows), we can estimate the overall similarity $AMI(i, j)$ and nodal modular variability $MV_k(i, j)$ between each pair of modular structures i and j , $i, j = 1, 2, \dots, n$. Then, for each node k , the total modular variability across all of the n partitions can be evaluated as (Steen et al., 2011):

$$MV_k = \sum_{i=1}^n w_i MV_k(i), \quad (6)$$

where $MV_k(i) = \sum_{j \neq i} MV_k(i, j) / (n-1)$ denotes the modular variability for node k between modular partition i and all of the other partitions. Notably, a normalized weight coefficient w_i is considered in the sum formula (6) to reduce the bias of potential outlier subjects or time

windows. For instance, if modular partition i dramatically differs from other partitions, the coefficient w_i will be assigned a small value. To be consistent with the overall analysis level, the weighted coefficient w_i was estimated using the AMI index for each modular structure i instead of the Jaccard similarity used in (Steen et al., 2011).

Inter- and intra-subject variability in modular organization

Using the above-mentioned network modular comparison approaches, we tracked the differences in the modular organization across subjects and within subjects at both overall and nodal levels. For the inter-subject modular variability analysis, the set of modular partitions in formula (6) represented the 105 static modular structures of all subjects, whereas for the intra-subject temporal modular variability analysis, the set of modular partitions in formula (6) represented the 1062 dynamic modular structures of each subject. For the latter analysis, we obtained a map of nodal modular variability for each subject, which was further averaged across subjects to depict the intra-subject modular variability in dynamic modular organization at the group level.

Reproducible pattern analysis of individual modular brain structures

To explore whether the brain's modular architecture and its temporal features were reproducible at an individual level across repeated sessions (i.e., S1 and S2), we proposed the following recurring pattern analysis procedure. Briefly, for two runs from S1 to S2, given an individual person of interest, we evaluated the within-subject recurrence of the modular organization by calculating the spatial similarity of the modular architectures of this subject in two sessions (S1 to S2). Then, we estimated the between-subject recurrence of the modular organization of this subject by calculating the spatial similarity values of the modular architecture of this subject in S1 against the modular architectures of all other subjects in S2 and taking the average value. We performed the same analysis for each subject and obtained within- and between-subject recurrence values for each subject. If the within-subject recurrence is significantly larger than the between-subject recurrence, the modular organization is considered to be reproducible at an individual level. The significant difference between within- and between-subject similarities was assessed across all subjects using a non-parametric permutation test, during which we randomly shuffled the subject identities for each session prior to the recurrence estimation. This permutation was repeated 10,000 times. Here, we examined the reproducible patterns for both the static modular structure and the intra-subject dynamic modular variability map, and the spatial similarity between two sessions was estimated using the AMI index and Pearson's correlation, respectively. Using the above-mentioned procedure, we also analyzed the reproducible pattern from S2 to S1.

Relationship with functional systems and cognitive flexibility

Previous studies suggested that the individual differences in intrinsic brain functional organization are heterogeneous across the brain (Finn et al., 2015; Langs et al., 2016; Mueller et al., 2013). Thus, it is important to examine whether and how the inter- and intra-subject modular variability varied across brain regions and the potential functional roles. First, we examined whether the inter-subject modular variability was dependent on the functional system. Given the eight major functional modules identified at the group level (Fig. 2A, left), including the visual, sensorimotor, default-mode, fronto-parietal, dorsal attention, ventral attention, limbic and subcortical modules, a one-way analysis of variance (ANOVA) was conducted on the modular variability values of the nodes within these modules to assess the effects of the functional module affiliations. Post hoc two-sample t-tests were also performed to assess the significant differences in modular

variability between any two modules. Second, we assessed the spatial similarity of the inter-subject and intra-subject modular variability maps by calculating Pearson's correlation coefficient across nodes. Third, to explore whether the inter- and intra-subject modular variability were associated with the regional functional connection profiles, we calculated their spatial correlations with the participation coefficients at the group level. The nodal participation coefficients at the group level were obtained by averaging the individual participation coefficients across subjects and reflected the spatial layout of the nodal functional connections among distinct modules (Guimera et al., 2005; He et al., 2009; Power et al., 2013). Finally, we compared the regional inter- and intra-subject modular variability with the number of cognitive components, which reflects the regional cognitive flexibility (Yeo et al., 2015) (https://surfer.nmr.mgh.harvard.edu/fswiki/BrainmapOntology_Yeo2015). For each nodal region, we estimated its cognitive flexibility by calculating the average number of cognitive components of all voxels within this node (Bertolero et al. 2015), and then calculated the spatial correlation between nodal cognitive flexibility and inter-/intra-subject modular variability.

Validation analysis

We evaluated whether the main findings were affected by the scanning sessions or different analysis strategies (including the parcellation scheme, module detection algorithm, network density and window length). The relevant procedures are described as follows. (i) Scanning session. To validate our main findings, we performed the same network module analysis on the R-fMRI data in the second session of the same subjects (i.e., S2). (ii) Parcellation scheme. Given that the topological organization of the brain networks could be affected by different ROI definitions (Fornito et al., 2010; Wang et al., 2009), we also constructed functional brain networks using two additional whole-brain parcellation schemes, including the Shen-268 (Finn et al., 2015; Shen et al., 2013) consisting of 268 ROIs and the Craddock-200 (Craddock et al., 2012) consisting of 200 ROIs. Both of these parcellation schemes are obtained from the population-level R-fMRI data through the clustering analysis, to ensure the functional homogeneity of the voxels within the same ROI. The ROIs in the brainstem were not considered in our analysis. (iii) Module detection algorithm. To date, several module detection algorithms are currently available with different advantages (Fortunato, 2010; Meunier et al., 2010; Sporns and Betzel, 2016). To investigate the potential effects of the module detection algorithms, we validated our main results using two additional popular methods, including the Louvain algorithm (Blondel et al., 2008) and the spectral optimization algorithm (Newman, 2006). (iv) Network density. During the functional network construction, we used a single network density ($S=15\%$) to ensure the same number of connections across all individuals and all sliding windows. To determine whether our main results depended on the choice of network density, we conducted analyses at two additional densities ($S=10\%$ and $S=20\%$). (v) Window length. To date, the optimal selection of the window length and the methodological pitfalls are not fully understood (Hindriks et al., 2015; Hutchison et al., 2013a; Leonardi and Van De Ville, 2015; Zalesky and Breakspear, 2015). In addition to the window length of 100 s, two additional window lengths (50 s and 150 s) were considered to validate the main results.

Influence of head motion and sampling error on intra-subject dynamic modular variability

A recent R-fMRI study demonstrated that dynamic functional connectivity fluctuations based on a sliding window-based approach were largely driven by sampling error and head motion (Laumann et al., 2016). To explore the potential influence of these two factors on the dynamic modular reconfigurations, we performed the following analyses.

Effects of head motion

To take into account of transient head motion, we performed an additional spike-regression-based scrubbing to the procedures of linear detrend and nuisance regression during R-fMRI data preprocessing (Power et al., 2015; Yan et al., 2013). Briefly, for each subject we first identified the “bad” volumes (i.e., time points) with framewise displacement (FD) above 0.2 mm and their adjacent volumes (1 back and 2 forward), and then modeled each “bad” time point as a separate regressor in the original regression models of linear detrend and nuisance regression. Subjects who had “bad” volumes in more than 40% of the original data in any of two sessions were excluded in the analysis. Finally, we reanalyzed the intra-subject modular variability based on the preprocessed data with additional head motion control for both sessions.

Effects of sampling error

In this study, for each subject we used a sliding window approach to generate 1062 dynamic brain connectivity matrices based on R-fMRI data. To assess the potential effects of sampling error, we proposed a null model to generate 1062 surrogate dynamic connectivity matrices. Specifically, for every surrogate matrix, the correlation coefficient of each edge was randomly assigned with one of the empirically observed 1062 correlation values of the corresponding edge. This random sampling procedure ensures that each edge of these surrogate matrices preserved the same correlation distribution as that of the empirical matrices. It is worthy to point out that for every surrogate matrix we randomly sampled each edge independently, rather than sampled one whole connectivity matrix from the empirical data. Thus, this null model can eliminate the potential across-time covariation of surrogate connections, thus yielding fully randomized sampling. Using this procedure, for each subject we constructed surrogate dynamic functional networks and generated the surrogate intra-subject modular variability map, followed by a comparison with the empirical data. To reduce the potential confounding effects of head motion, this null model was performed on the subjects with additional head motion control mentioned above.

Results

Static modular architecture across individuals

At the group level, the static brain network was decomposed into eight major functional modules: the default-mode, sensorimotor, visual, fronto-parietal, ventral attention, dorsal attention, subcortical and limbic modules (Fig. 2A, left). The modular structure was largely consistent with the functional systems shown in several previous studies (He et al., 2009; Power et al., 2011; Yeo et al., 2011). At an individual level, the number of modules ranged from 3 to 8 (mean \pm std=5.36 \pm 0.98) and the functional modular structure of each subject was generally similar to the structure observed at the group level (AMIs, mean \pm std=0.31 \pm 0.07) (Fig. 2A, right). However, there were some remarkable differences in regional modular affiliations across individuals (AMIs, mean \pm std=0.21 \pm 0.06) (Fig. 2B). Notably, the inter-subject variability in module affiliations was non-homogeneous across the brain, with the most obviously variable regions located primarily at the middle frontal gyrus, intraparietal sulcus, anterior/middle cingulate cortex, anterior insula, and medial temporal lobe as well as the thalamus and putamen (Fig. 2C, left). Furthermore, based on the group-level modular structure, we found that the inter-subject variability was significantly different among functional modules (one-way ANOVA, $F_{(7,248)}=51.83$, $p < 0.0001$), with significantly higher values in the fronto-parietal, dorsal and ventral attention, limbic and subcortical systems compared to the default-mode, sensorimotor and visual systems (post-hoc t -tests, all $ps < 0.05$, Bonferroni corrected) (Fig. 2C, right).

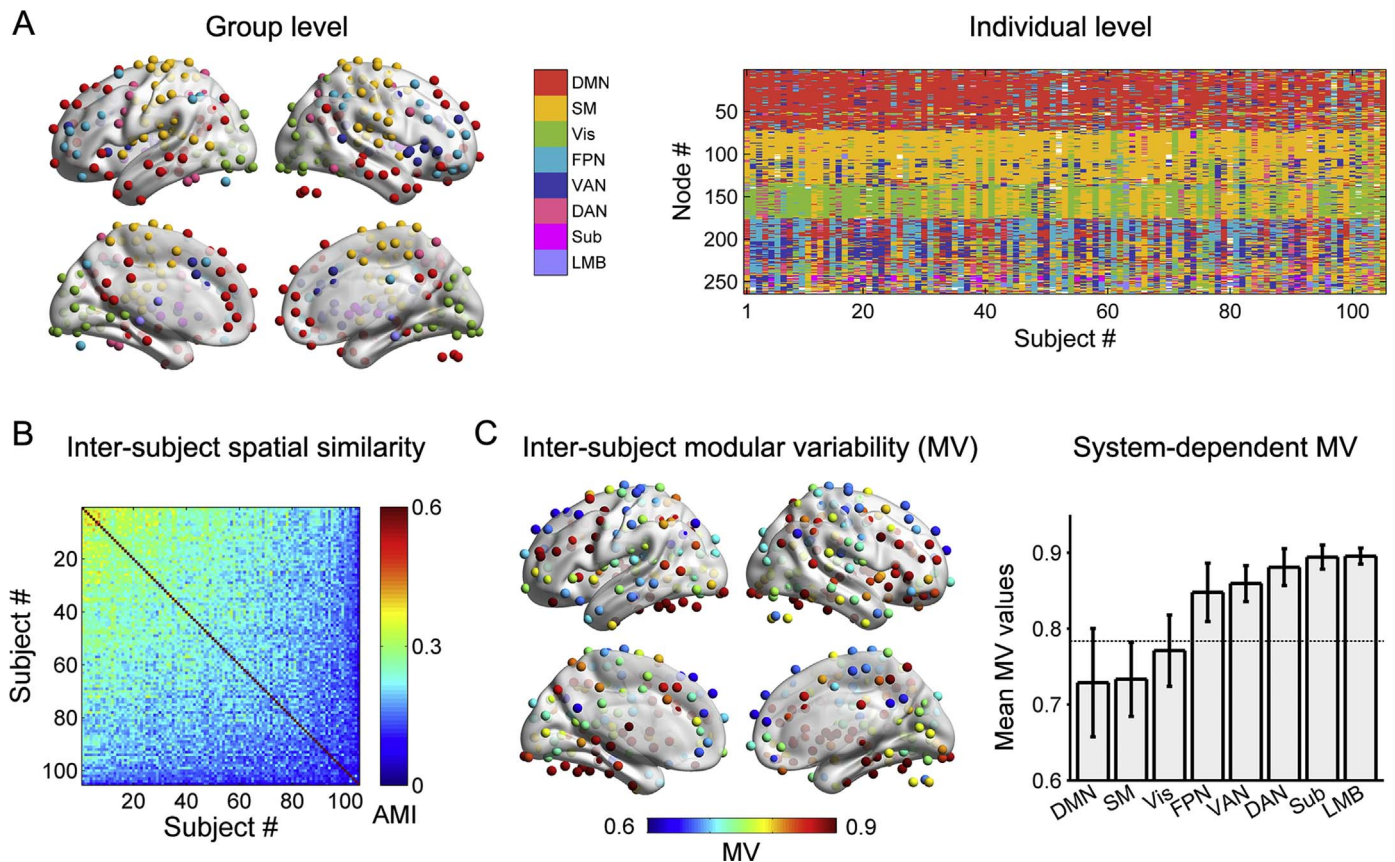


Fig. 2. Static modular structures and their inter-subject variability. (A) Modular structures at the group level (left panel) and at the individual level (right panel). Eight major modules were identified at the group level, and modules with fewer than five nodes are not shown. Individual modular structures were matched to the group level structure for better visualization using the Hungarian matching algorithm (Kuhn 1955), and the modules not belonging to the eight major modules were colored white. (B) Inter-subject spatial similarity of the modular structures estimated using adjusted mutual information (AMI). (C) Inter-subject modular variability in the whole brain (left panel) and within the eight functional modules obtained at the group level (right panel). For each node, the inter-subject variability in the module affiliation was estimated using modular variability (MV). The dashed line in the right panel denotes the mean MV value across the brain. The nodes were mapped onto the cortical surfaces using the BrainNet Viewer package (Xia et al., 2013). DMN, default-mode; SM, sensorimotor; Vis, visual; FPN, fronto-parietal; VAN, ventral attention; DAN, dorsal attention; Sub, subcortical; LMB, limbic.

Dynamic modular architecture within and across individuals

For each subject, we observed that the network nodes dynamically switched their module affiliations across time windows, suggesting a time-dependent modular structure of the brain networks. Fig. 3A displays the dynamic reconfiguration of modular structures for one representative subject, where the modularity fluctuated in a range from 0.32 to 0.53 (mean \pm std = 0.44 ± 0.04), and the number of modules varied from 3 to 8 (mean \pm std = 5.59 ± 0.97). Although the modular structures were slightly modulated in neighboring windows (AMIs, mean \pm std = 0.82 ± 0.10), the structures in non-adjacent windows exhibited relatively lower similarities (AMIs, mean \pm std = 0.24 ± 0.13) (Fig. 3A, right). The temporal variability in module affiliations across all time windows was spatially heterogeneous, with large variability predominantly located in the prefrontal, inferior parietal and medial temporal cortices as well as several subcortical regions (Fig. 3B, left). Moreover, an averaged map across individuals indicated that these regions also exhibited large temporal variability at the population level (Fig. 3B, right). Interestingly, this temporal modular variability map that captured dynamic modular reorganization was very similar to the inter-subject modular variability map capturing changes in the static modular structure ($r=0.82$, $p < 0.0001$) (Fig. 3C).

Reproducible modular brain architecture across sessions

For the static modular structure, we observed that the across-session spatial similarity within the same subject (AMIs, mean \pm

std = 0.36 ± 0.09) was significantly higher than the similarity between different subjects estimated from either S1 to S2 (AMIs, mean \pm std = 0.21 ± 0.03) or the reverse (AMIs, mean \pm std = 0.21 ± 0.03) (permutation tests, both $ps < 0.001$, Bonferroni corrected) (Fig. 4A). When considering the dynamic modular reconfiguration, we examined the across-session reproducibility of the intra-subject modular variability maps. We found that the across-session spatial similarity within the same subject (rs , mean \pm std = 0.45 ± 0.22) was significantly higher than the similarity between different subjects estimated from either S1 to S2 (rs , mean \pm std = 0.22 ± 0.08) or the reverse (rs , mean \pm std = 0.22 ± 0.07) (permutation tests, both $ps < 0.001$, Bonferroni corrected) (Fig. 4B). These findings indicate that both the static modular structures and intra-subject modular variability maps were reproducible at an individual level across different scanning sessions.

Relationship with functional connectors and cognitive flexibility

First, the across-node correlation analysis revealed that the mean participation coefficient map obtained at the group level exhibited significant correlations with both the inter-subject static modular variability and the mean intra-subject dynamic modular variability maps (Fig. 5A, inter-subject variability, $r=0.90$, $p < 0.0001$; mean intra-subject variability, $r=0.81$, $p < 0.0001$). Second, visual examination indicated that these modular variability maps (Fig. 2C and Fig. 3B, right) were remarkably similar to the regional cognitive flexibility map (Fig. 5B, left) (Yeo et al., 2015). The across-node correlation analysis revealed that the number of cognitive components significantly in-

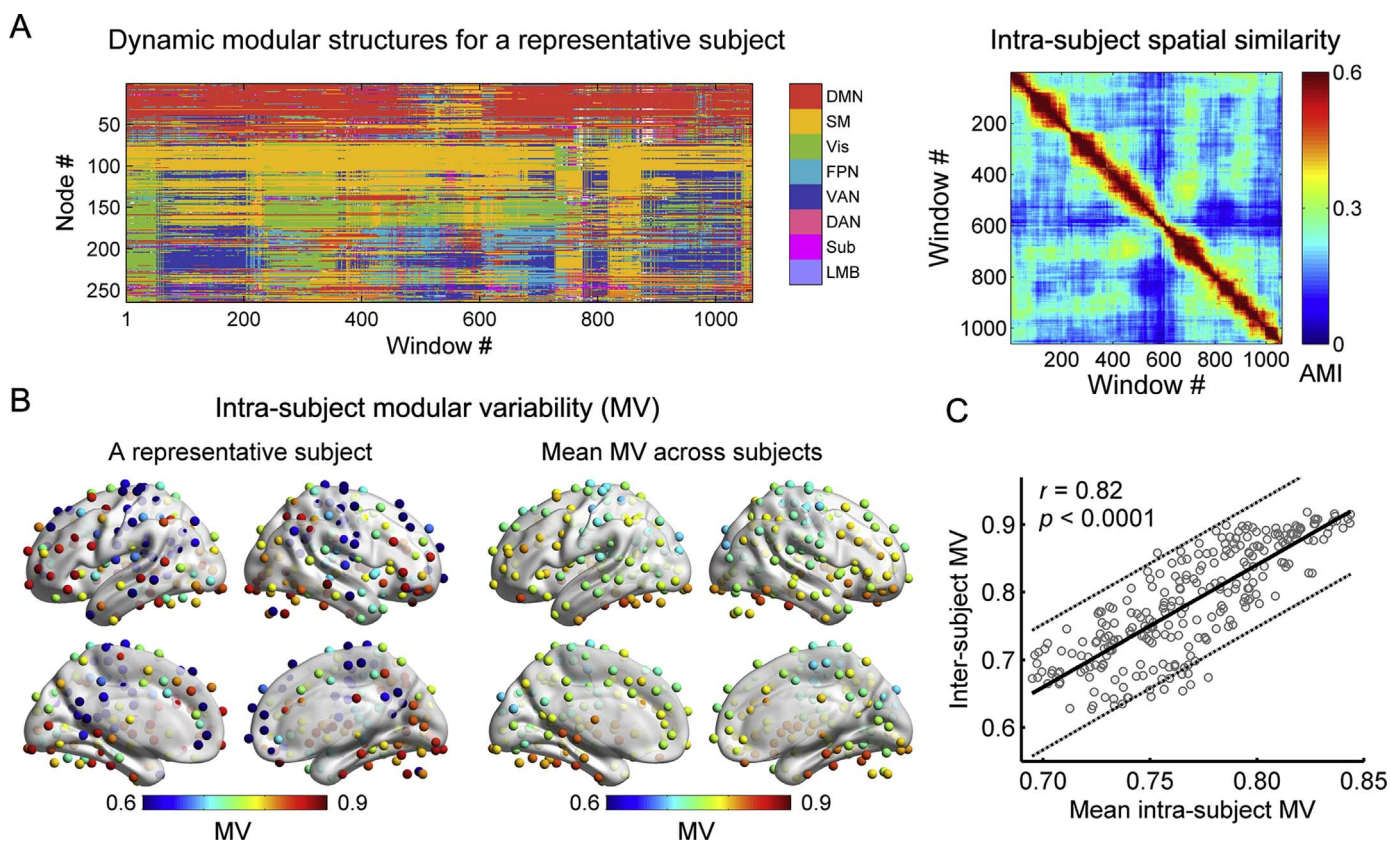


Fig. 3. Dynamic modular structures over time and intra-subject modular variability. (A) Dynamic modular structures (left panel) and their spatial similarity (right panel) for a representative subject. For better visualization, the functional modules in each time window were matched to the group level modules (Fig. 2A, left panel) using the Hungarian matching algorithm (Kuhn, 1955), and the modules not belonging to the eight major modules were colored white. (B) Intra-subject modular variability for a representative subject (left panel) and the whole group (right panel). For each node, the temporal variability in module affiliations over time was estimated using modular variability (MV). The temporal modular variability map for the whole group was generated by averaging individual maps across subjects. (C) Across-node relationship between the inter-subject modular variability and the mean intra-subject modular variability across subjects. The dotted lines in the scatter plot denote the 95% prediction error bounds, hereinafter the same.

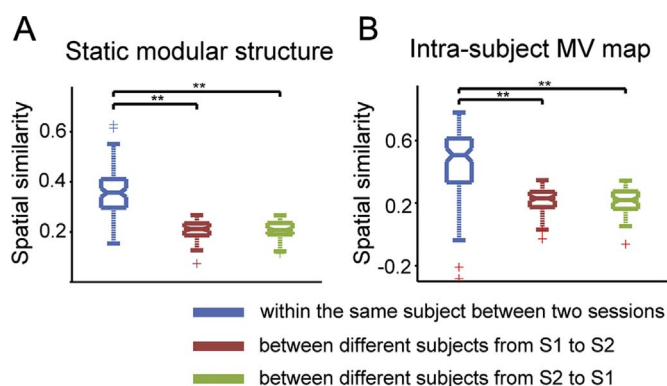


Fig. 4. Spatial similarity of static modular structures (A) and intra-subject modular variability maps (B) between two sessions. For each subject, we calculated the spatial similarity within the same subject between two sessions (blue), the mean spatial similarity of the modular feature of this subject in S1 with the modular features of all the other subjects in S2 (red), and the mean spatial similarity of the modular feature of this subject in S2 with the modular features of all the other subjects in S1 (green). The spatial similarity between two static modular structures was estimated using the AMI index, and the spatial similarity between two intra-subject modular variability maps was estimated using Pearson's correlation. Significant differences between different categories were tested using permutation tests (** $p < 0.001$, Bonferroni corrected). AMI, adjusted mutual information.

creased with either inter-subject or mean intra-subject modular variability (Fig. 5B, inter-subject variability, $r=0.42$, $p < 0.0001$; intra-subject variability, $r=0.25$, $p < 0.0001$). All of these results suggest

that the regions exhibiting higher modular variability across subjects or over time tend to be functional connector hubs linking multiple brain systems and engage in multiple cognitive components.

Validation results under different network analysis strategies

We validated our main findings using data from another scanning session (S2) (Figs. 6A and S1) and different analysis strategies, involving parcellation schemes (Figs. 6B and 6C), module detection algorithms (Fig. S2), network densities (Fig. S3) and sliding window lengths (Fig. S4). We found that the spatial patterns of both inter-subject modular variability and mean intra-subject modular variability were highly reproducible between two scanning sessions and across different analysis strategies (Fig. S5) and the main findings replicated well regardless of the scanning session and analysis strategy used (Table 1). Interestingly, we found that the intra-subject temporal modular variability increased with the decreasing network density and window length while maintaining high spatial similarity with the inter-subject modular variability.

Influence of head motion on intra-subject dynamic modular variability

For 105 subjects used in the main analyses, the mean FD across time for each subject ranged from 0.08 to 0.28 mm (mean \pm std = 0.16 ± 0.04 mm) (Fig. S6). After an additional operation of spike-regression-based scrubbing, 17 subjects were remained due to our very stringent criterion of bad time points, and most results regarding intra-subject modular variability remained very little changed. Specifically, for these

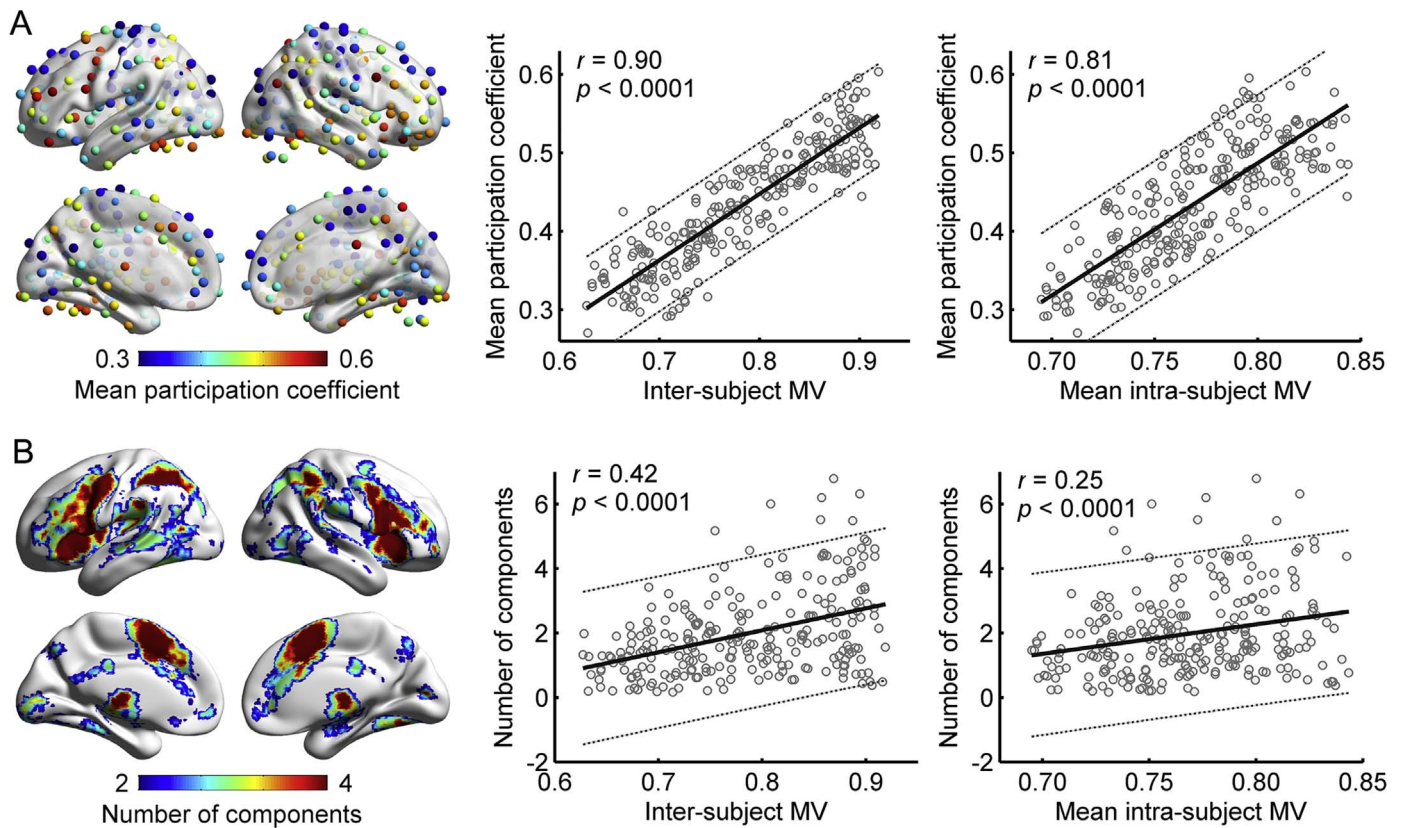


Fig. 5. Relationship with participation coefficients and cognitive flexibility. (A) Mean participation coefficient across subjects (left panel) and the cross-node relationship with inter-subject modular variability (middle panel) and the mean intra-subject modular variability across subjects (right panel). (B) Number of cognitive components adapted from Yeo et al. (2015) (left panel) and their relationships with inter-subject modular variability (middle panel) and the mean intra-subject modular variability across subjects (right panel). For each nodal region, we estimated its cognitive flexibility by averaging the cognitive component numbers of all voxels within this node. MV, modular variability.

subjects, the subject-specific spatial patterns of intra-subject modular variability were highly similar before and after data scrubbing (spatial correlation, $r_s > 0.92$ for all subjects). Additionally, the group-level intra-subject modular variability map for these 17 subjects showed high spatial similarity with that of all 105 subjects without data scrubbing (Fig. 7A: $r = 0.92$, $p < 0.0001$), although the average value across the brain was a little decreased after data scrubbing (for 17 subjects with data scrubbing, average value's range: 0.62–0.81, mean \pm std = 0.76 ± 0.05 ; for 105 subjects without data scrubbing, average value's range: 0.62–0.83; mean \pm std = 0.77 ± 0.04). Similar results were also observed in Session 2 (not shown).

Influence of sampling error on intra-subject dynamic modular variability

We generated the surrogate dynamic connectivity matrices for the 17 subjects with additional head motion control. Based on the Infomap algorithm, the intra-subject modular variability maps were obtained only in 10 subjects since the probabilities to find a significant modular architecture in the surrogate networks were below 50% for other 7 subjects. For these 10 subjects, the mean intra-subject modular variability across the brain ranged from 0.62 to 0.78 (mean \pm std = 0.73 ± 0.05) in the empirically observed brain networks (i.e., R-fMRI data), while ranging from 0.11 to 0.41 (mean \pm std = 0.28 ± 0.09) in the surrogate data obtained from the null model (Fig. 7B). By performing paired t-test analyses across nodes, for each subject we found that the magnitude of intra-subject modular variability in the empirically observed brain networks was significantly higher than that in the surrogate data (all $p_s < 0.001$, Bonferroni corrected).

Discussion

Using multiband R-fMRI data from a large population and graph-based network modularity analysis, we demonstrated the individual variability and dynamic reconfiguration of intrinsic modular architectures in resting human brain networks. Our main findings are as follows. First, we found that the intrinsic modular structures exhibited remarkable differences across individuals, primarily involving the heteromodal association cortex (e.g., fronto-parietal system) and the subcortical areas. Importantly, these regions also substantially changed their module affiliations over time on a time scale of seconds. Second, the intrinsic modular architectures and their temporal characteristics were well reproducible across scanning sessions at an individual level. Third, the regions with large module affiliation variability were closely associated with the functional connectors and cognitive flexibility. Fourth, the remarkable intra-subject dynamic modular variability observed here cannot be fully explained by the head motion and sampling error. Finally, the main findings remained largely unchanged regardless of the parcellation schemes and the module detection algorithms considered. We discuss these findings in more detail in the following sections.

Individual variability in intrinsic modular structures

Most previous studies on functional modular architecture focused on the functional modules at the population level (He et al., 2009; Meunier et al., 2009; Power et al., 2011), which might reflect the general organization principles in a population. Consistent with these previous studies, we identified functionally specialized but interacting functional modules at the population level, such as the sensorimotor,

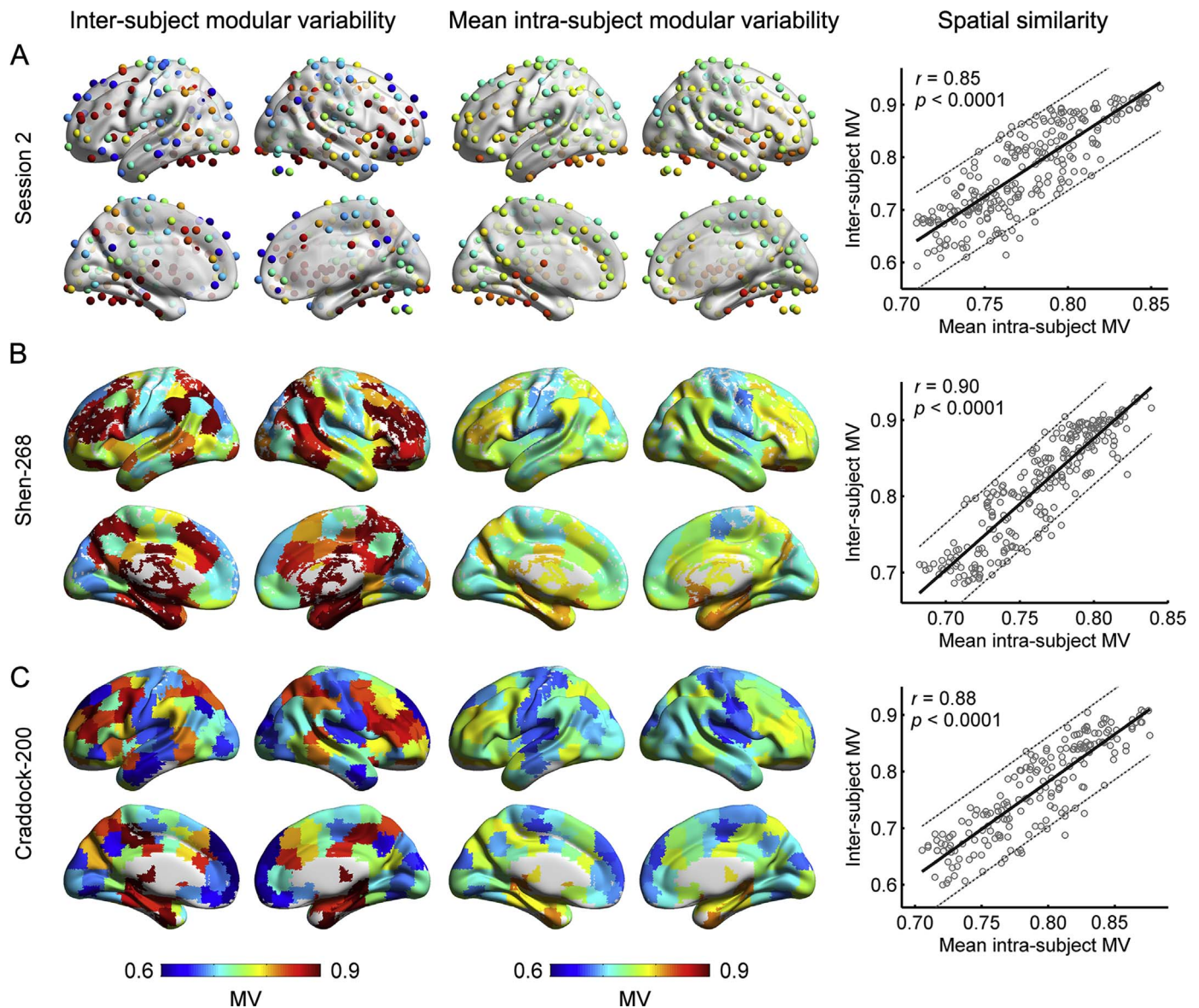


Fig. 6. Inter- and mean intra-subject modular variability maps and their spatial similarity under different conditions. (A) Inter- and mean intra-subject modular variability obtained from the R-fMRI data in Session 2 of the same participants. (B) Inter- and mean intra-subject modular variability in functional networks obtained via the Shen-268 parcellation scheme (Finn et al., 2015; Shen et al., 2013). (C) Inter- and mean intra-subject modular variability in functional networks obtained via the Craddock-200 parcellation scheme (Craddock et al., 2012). MV, modular variability.

visual, default-mode, fronto-parietal, attention and subcortical systems. However, when observing the modular brain structures at an individual level, we found that the individual modular brain structures exhibited substantial differences from one another, and that the inter-subject modular variability was spatially inhomogeneous. More specifically, the primary and default-mode modules were relatively consistent across individuals, whereas several heteromodal association cortical areas (e.g., bilateral frontal and parietal areas, and medial temporal lobe) and subcortical areas (e.g., thalamus and putamen) exhibited larger inter-subject modular variability. These findings are largely consistent with a previous study demonstrating highly similar default-mode, sensorimotor and visual modular structures across subjects (Moussa et al., 2012). Besides, high individual variability of network membership predominantly in association areas was also reported for functional parcellation/system comparisons across individuals (Gordon et al., 2015; Langs et al., 2016) and functional module comparisons between a single individual and a group average (Laumann et al., 2015), which provided further support for our findings. Of note, several subjects had a small number of modules

(e.g., 3) in the static brain networks, possibly due to the network density considered. As the network density decreases, more modules could be observed in the human brain networks (Power et al., 2011). Another possible reason was that these subjects underwent specific scanning status in which different brain systems were highly integrated through some unexpected connections, leading to a small number of network modules.

As suggested in very recent studies (Bertolero et al., 2015; Yeo et al., 2015), functional modules may perform discrete cognitive function that are reused in different cognitive tasks. Thus, cross-module communication is of crucial importance for individual cognition and behavior. Because the heteromodal association areas are largely responsible for information integration and coordination across distributed regions (Bertolero et al., 2015; Power et al., 2013), it is natural to expect that these regions may be functionally different across individuals to partially account for individual differences in cognitive performance. In support of this notion, we found that the highly variable regions observed here were usually functional connectors connecting multiple modules, as evidenced by the strong correlation

Table 1
Reproducibility of main findings under different analysis strategies.

Analysis strategy	Inter-subject MV vs. Mean intra-subject MV	Mean participation coefficient		Number of components	
		Inter-subject MV	Mean intra-subject MV	Inter-subject MV	Mean intra-subject MV
S1	0.82	0.90	0.81	0.42	0.25
S2	0.85	0.94	0.84	0.42	0.24
Louvain	0.87	0.86	0.74	0.44	0.31
Newman	0.86	0.85	0.75	0.44	0.29
10%	0.85	0.72	0.38	0.46	0.31
20%	0.74	0.91	0.90	0.39	0.19
50 s	0.76	0.90	0.76	0.42	0.22
150 s	0.85	0.90	0.84	0.42	0.27

All functional networks were constructed using a functional atlas consisting of 264 nodes (Power et al., 2011) based on R-fMRI in the first session (i.e., S1), except the strategy denoted by S2. The mean participation coefficients were generated by averaging individual participation coefficients in static functional networks across subjects. The numbers of cognitive components were extracted from Yeo et al. (2015). The mean intra-subject MV values were obtained by averaging the intra-subject MV maps across subjects. The spatial correlation between the inter-/intra-subject MV and the participation coefficient as well as the number of cognitive components were estimated using Pearson's correlation analysis across nodes. Significant correlations were observed in all cases (all p s < 0.01). MV, modular variability.

with the participation coefficients (Fig. 5A), and thus tended to show high cognitive flexibility (Fig. 5B). Of note, as known individual differences in the anatomical layouts of functional systems (Frost and Goebel, 2012; Gordon et al., 2015; Langs et al., 2016), employing a group-level parcellation scheme may induce some nodes sitting on the module borders. These nodes may blur signals from multiple functional systems and thus tend to exhibit larger inter-subject variability and higher participation coefficients. To assess the potential influence of this issue, we re-estimated the correlation between inter-subject modular variability and participation coefficients with correcting for the functional homogeneity of nodes. We found that the spatial correlation changed very little from 0.849 to 0.846 after correcting for nodal homogeneity indices for the subjects with additional head motion control (Fig. S7), indicating that the high spatial correlation between inter-subject modular variability and the participation coefficients cannot be primarily explained by the signal blurring in some nodes for some subjects.

The high inter-subject modularity variability of these regions may be attributable to individual differences in their functional connectivity patterns with other brain areas (Laumann et al., 2015; Mueller et al., 2013). During human development, the association cortical areas undergo protracted maturation during the high plasticity postnatal period (Casey et al., 2005; Hill et al., 2010b; Petanjek et al., 2011), which may be shaped by their phylogenetically late-development during evolution (Buckner and Krienen, 2013; Clancy et al., 2000; Van Essen and Dierker, 2007). Therefore, the higher functional variability observed for the association areas may be due to their prolonged exposure to environmental factors that vary across individuals (Mueller et al., 2013; Zilles and Amunts, 2013). Additionally, several subcortical regions (e.g., thalamus and putamen) also exhibited high inter-subject modular variability, which might be explained by their extensive weak functional connectivities for information integration across distributed brain regions (Cole et al., 2010). Although the physiological sources for the inter-subject modular variability remain largely unknown, we believe that identification of the functional modules in an individual and discernment of their individual differences might provide a novel neural underpinning for individual cognition and behavior.

Dynamic modular organization in the resting-state

Recent R-fMRI studies revealed that the functional organization of the human brain undergoes dynamic reconfiguration on a time scale of seconds during rest (Calhoun et al., 2014; Hutchison et al., 2013a). In the current study, we identified the dynamic changes of functional modular organization at both overall and nodal levels using a commonly used sliding window approach. At the overall level, the modularity and number of modules varied over time, implying the dynamic adjustment of information segregation and integration over time, which was compatible with previous studies (Allen et al., 2014; Betzel et al., 2016; Di and Biswal 2015; Jones et al., 2012). Interestingly, for a given subject, relatively small module numbers (e.g., 3 modules, Fig. 3A) were observed at some specific windows, even at a fixed network density. This could be partially attributable to the fact that certain connections were unexpectedly strong at some time windows (Betzel et al., 2016) and thus tightly integrated different functional systems. At the regional level, we found that the brain regions showed dynamic module affiliations, which extended our previous understanding regarding the dynamic functional connectivity profiles (Zhang et al., 2016) or connectivity degrees (Liao et al., 2015) and might reflect a temporal switch of functional roles or functional flexibility for the regions. These temporal changes in functional modules may be partially explained by the shift of arousal/vigilance states (e.g., increasing tendency of drowsiness) during the unconstrained resting state (Allen et al., 2014; Calhoun et al., 2014; Laumann et al., 2016), as supported by spontaneous eyelid closures during rest (Wang et al., 2016). Nevertheless, the dynamic modular reconfigurations may also partly manifest inherent brain dynamics as demonstrated in the anesthetized macaque brain (Hutchison et al., 2013b). Using computational models naturally free from physiological artifacts (Deco et al., 2011; Deco et al., 2013; Haimovici et al., 2013; Hansen et al., 2015) and empirical R-fMRI studies (Liu and Duyn, 2013; Tagliazucchi et al., 2012a), researchers pointed out that the human brain might reside near a critical/subcritical state that allows the existence of a rich repertoire of functional configurations. These time-resolved functional modules may reflect the spontaneous transitions among the potential functional coordination configurations, which promote the fast response to extrinsic cognitive demands (Deco et al., 2011; Deco et al., 2013).

Interestingly, the regions showing dramatic temporal variability largely overlapped those exhibiting remarkable inter-subject modular variability (Fig. 3C and Fig. 6), suggesting a potential contribution to individual differences. Previous task-fMRI studies have reported that the functional connectors (e.g., fronto-parietal areas) may frequently switch between different functional modules during the task performance for better flexibility and higher cognitive performance (Bassett et al., 2011; Bassett et al., 2013; Bassett et al., 2015; Braun et al., 2015). Here, by unveiling the significant relation between regional temporal modular variability and cognitive flexibility (Fig. 5B), we demonstrated that the region-dependent dynamic module affiliations during rest might form the intrinsic functional foundation for individual flexible cognitive function. Through a ROI-wise across-subject correlation analysis (Fig. S8), we observed significant positive correlation between intra-subject modular variability and individual fluid intelligence (here, PMAT24_A_CR score) at two ROIs separately locating at left medial prefrontal cortex and right supplementary motor areas, regardless the analysis strategies considered ($p < 0.05$, uncorrected for multiple comparisons). These two regions were in good accordance with previously identified intelligence-related regions (Jung and Haier, 2007), indicating the behavior relevance of the intra-subject modular variability. As we only considered bivariate Spearman's correlations in this exploratory analysis, several other models can be considered in the future to better reveal the complex relationship between dynamical modular organization and individual cognitive performance.

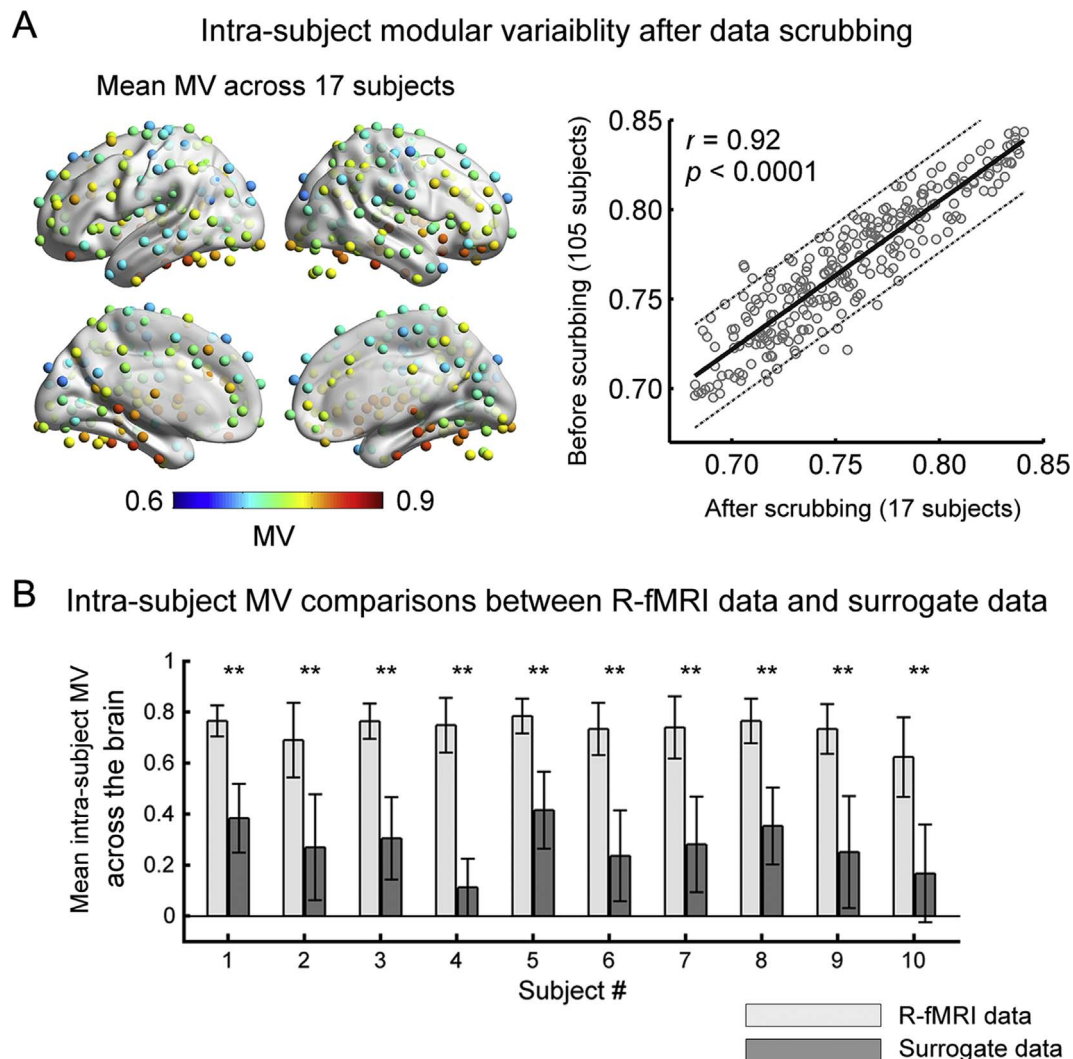


Fig. 7. Intra-subject dynamic modular variability in R-fMRI data with data scrubbing and in surrogate data. (A) Group-level intra-subject modular variability map for 17 subjects with a scrubbing procedure for head motion correction (left panel) and its spatial similarity with that of 105 subjects without data scrubbing (right panel). (B) Mean intra-subject modular variability across the brain and the corresponding standard deviation within each subject for both R-fMRI data and surrogate data. For each subject, significantly higher regional intra-subject modular variability was observed in R-fMRI data in comparison with surrogate data through a paired t-test across nodes (** $p < 0.001$, Bonferroni corrected). MV, modular variability.

Individual-specific modular structures

Exploring individual differences in functional brain organization from spontaneous brain activities can provide neural mechanisms underlying human cognition and behavior (Dubois and Adolphs, 2016; Kelly et al., 2012). Recent studies demonstrated that the regional and whole-brain functional connectivity patterns varied across individuals (Finn et al., 2015; Mueller et al., 2013), which might be regarded as the “fingerprint” to distinguish one individual from another. Here, we found that subject-specific spatial patterns of both the intrinsic modular structures and the intra-subject modular variability maps were reproducible across different scanning sessions, with a significantly larger spatial similarity between the same subjects than that between different subjects (Fig. 4). These findings extend previous results regarding individual variability in functional connectivity patterns (Finn et al., 2015; Mueller et al., 2013), and indicate that the intrinsic modular structures at rest can make contribution to individual identification. Of note, low spatial similarity between sessions was also observed in intra-subject modular variability maps for a few subjects (e.g., outliers in Fig. 4B, right), which may be attributable to their different fluctuating vigilance levels between two scanning sessions (Allen et al., 2014; Laumann et al., 2016; Wang et al., 2016).

Given that the intrinsic functional modules identified at rest show a spatial correspondence with the task-evoked activity in meta-analyses (Bertolero et al., 2015; Crossley et al., 2013; Power et al., 2011; Smith et al., 2009), the individual differences in the modular structure at rest may be associated with the inter-subject variability in the task-evoked activities (Frost and Goebel 2012) and thus provide novel insights into individual differences in cognition and behavior. Additionally, exploring the alteration of the modular structures and their dynamic features may be suggestive for neurological and psychiatric disorders, especially for those involving the impairments of higher-order cognitive function.

Effects of head motion on dynamic characteristics

During the data preprocessing, we have performed strict head motion control to reduce the influence of head motion. Specifically, we excluded subjects with large head motion and further included the 24 head motion parameters (Friston et al., 1996) and global signal as regressors during nuisance regression (Yan et al., 2013). When performing an additional spike-regression-based scrubbing (Power et al., 2015; Yan et al., 2013), our main results remained almost unchanged. These findings suggest that the remarkable intra-subject modular variability observed here was not dominantly driven by the

head motion. Notably, Laumann et al. (2016) also observed a small but evident excess of kurtosis in empirical data compared with simulated data, which could not be explained by head motion or fluctuating drowsiness. Together, our findings demonstrate the presence of remarkable dynamic functional organization after very stringent head motion control, suggesting that the dynamical modular organization is more than the head motion effects. Finally, it is worth mentioning that only 17 of 105 subjects were remained after stringent head motion controls, indicating a relatively high portion of “bad” volumes estimated in the HCP database. In line with our observations, Power (2016) also reported that the HCP data often exhibited high motion estimations. Although the exact reasons for the large head motion parameters were unknown, the influencing factors could be involved in the fast sampling rate or some sequence- or hardware-specific properties of the scans (Power 2016). As a recent study suggests a neurobiological basis underlying the head motion (Zeng et al., 2014), the correction and interpretation of head motion should be carefully handled in the future.

Effects of sampling error on dynamic characteristics

Here, we evaluated the potential influence of sampling error by generating surrogate data using a random sampling approach. In line with previous studies (Hindriks et al., 2015; Laumann et al., 2016), we found that sampling error indeed induced a certain degree of intra-subject modular variability (Fig. 7B). But more importantly, we found that for each subject the magnitude of intra-subject modular variability in the empirically observed brain networks was significantly larger than that in the surrogate data, indicating that the intra-subject modular variability during rest cannot be explained by sampling error. One possible explanation is that in empirical brain networks different connections may co-vary across windows in a coordinated manner, thus yielding large enough changes in functional correlation patterns that can be detected as modular reconfigurations. This speculation can be supported by a recent study showing that some specific connections were unexpectedly strong or weak at some time points and tended to cluster temporally (Betzel et al., 2016). In addition, growing evidence has demonstrated that the dynamical functional organization during rest exhibited electrophysiological (e.g., EEG) correlations (Chang et al., 2013; Tagliazucchi et al., 2012b; Zhang et al., 2016) and showed alterations in development and diseases (Damaraju et al., 2014; Hutchison and Morton, 2015; Li et al., 2014; Zhang et al., 2016). Together with these previous studies, our findings suggest that intra-subject modular variability observed here may partly reflect the intrinsic ongoing fluctuations of brain organization during rest.

Notably, several previous studies using a sliding window approach have observed significant temporal fluctuations in functional connections during rest in comparison with surrogate data (Betzel et al., 2016; Zalesky et al., 2014), but others not (Hindriks et al., 2015; Laumann et al., 2016). The divergent conclusions across different studies might be attributable to the different dynamic characteristics of interest and different null hypotheses used. For instance, Hindriks et al. (2015) focused on the linear and non-linear statistics of time-varying functional connectivity and generated surrogate data using a phase randomization procedure (Prichard and Theiler, 1994), whereas Zalesky et al. (2014) tested the non-linear properties of functional connectivity fluctuations and generated surrogate data using stable vector autoregressive null models. Besides, both studies of Hindriks et al. (2015) and Laumann et al. (2016) did not completely deny the presence of time-dependent functional interactions. Hindriks et al. (2015) argued that some functional connections are in fact dynamic when tested using session-/subject-average measures. Future studies should be carefully conducted when selecting an appropriate null hypothesis for statistical tests, as till now there is no golden standard on how to evaluate dynamic characteristics of functional organization during rest (Betzel et al., 2016; Hindriks et al., 2015).

Further considerations

Several issues need to be further considered. First, to address the potential effects of the module detection algorithms, we used the Louvain algorithm (Blondel et al., 2008) and the spectral optimization algorithm (Newman 2006) to validate our results, and our main findings were preserved. Because there is no clear standard regarding which algorithm is optimal for brain module detection, the suitability of different algorithms has yet to be established. Second, we obtained the main results using a functional atlas obtained from a combination of meta-analysis of task-fMRI and resting-state functional connectivity analysis (Power et al., 2011), which reduces the risks of signal blurring from multiple functional areas within a node at an individual level (Wig et al., 2011). Ideally, the nodes should be defined according to a subject-specific functional parcellation when analyzing individual differences. However, how to determine the optimal number of parcels for each subject and how to align parcels across subjects remain open questions (Wang et al., 2015a). In the future, exploring the modular variability across individuals and over time at a higher spatial resolution (e.g., single voxel or vertex) could be promising if the computing power allows. Finally, the incorporation of multimodal imaging data of the same subjects in future work, such as the structural, diffusion and functional MRI as well as magnetic resonance spectroscopy, will be important to explore the physiological and molecular basis underlying the inter-subject variability and the temporal characteristics of the intrinsic modular architecture.

Acknowledgments

We would like to thank Dr. Zhengjia Dai for valuable discussions. This work was supported by the National Key Basic Research Program of China (973) (Grant no. 2014CB846102), the National Natural Science Foundation of China (Grant nos. 91432115, 81620108016, 31521063, 81671767 and 81401479), the China Postdoctoral Science Foundation (Grant no. 2016T90056), Changjiang Scholar Professorship Award (Award no. T2015027), Beijing Municipal Science & Technology Commission (Grant nos. Z161100004916027, Z16110000216152 and Z151100003915082) and the Open Research Fund of the State Key Laboratory of Cognitive Neuroscience and Learning (Grant no. CNLYB1307). Data were provided by the Human Connectome Project, WU-Minn Consortium (Principal Investigators: David Van Essen and Kamil Ugurbil; 1U54MH091657) funded by the 16 NIH Institutes and Centers that support the NIH Blueprint for Neuroscience Research; and by the McDonnell Center for Systems Neuroscience at Washington University.

Appendix A. Supporting information

Supplementary data associated with this article can be found in the online version at doi:10.1016/j.neuroimage.2017.02.066.

References

- Allen, E.A., Damaraju, E., Plis, S.M., Erhardt, E.B., Eichele, T., Calhoun, V.D., 2014. Tracking whole-brain connectivity dynamics in the resting state. *Cereb. Cortex* 24, 663–676.
- Amunts, K., Schleicher, A., Burgel, U., Mohlberg, H., Uylings, H.B., Zilles, K., 1999. Broca's region revisited: cytoarchitecture and intersubject variability. *J. Comp. Neurol.* 412, 319–341.
- Amunts, K., Weiss, P.H., Mohlberg, H., Pieperhoff, P., Eickhoff, S., Gurd, J.M., Marshall, J.C., Shah, N.J., Fink, G.R., Zilles, K., 2004. Analysis of neural mechanisms underlying verbal fluency in cytoarchitectonically defined stereotaxic space—the roles of Brodmann areas 44 and 45. *Neuroimage* 22, 42–56.
- Anderson, M.L., 2014. Complex function in the dynamic brain: comment on "Understanding brain networks and brain organization" by Luiz Pessoa. *Phys. Life Rev.* 11, 436–437.
- Bassett, D.S., Yang, M., Wymbs, N.F., Grafton, S.T., 2015. Learning-induced autonomy of sensorimotor systems. *Nat. Neurosci.* 18, 744–751.
- Bassett, D.S., Wymbs, N.F., Porter, M.A., Mucha, P.J., Carlson, J.M., Grafton, S.T., 2011.

- Dynamic reconfiguration of human brain networks during learning. *Proc. Natl. Acad. Sci. USA* 108, 7641–7646.
- Bassett, D.S., Wymbs, N.F., Rombach, M.P., Porter, M.A., Mucha, P.J., Grafton, S.T., 2013. Task-based core-periphery organization of human brain dynamics. *PLoS Comput. Biol.* 9, e1003171.
- Bertolero, M.A., Yeo, B.T., D'Esposito, M., 2015. The modular and integrative functional architecture of the human brain. *Proc. Natl. Acad. Sci. USA* 112, E6798–E6807.
- Betz, R.F., Fukushima, M., He, Y., Zuo, X.N., Sporns, O., 2016. Dynamic fluctuations coincide with periods of high and low modularity in resting-state functional brain networks. *Neuroimage* 127, 287–297.
- Birn, R.M., Diamond, J.B., Smith, M.A., Bandettini, P.A., 2006. Separating respiratory-variation-related fluctuations from neuronal-activity-related fluctuations in fMRI. *Neuroimage* 31, 1536–1548.
- Biswal, B., Yetkin, F.Z., Haughton, V.M., Hyde, J.S., 1995. Functional connectivity in the motor cortex of resting human brain using echo-planar MRI. *Magn. Reson. Med.* 34, 537–541.
- Blondel, V.D., Guillaume, J.-L., Lambiotte, R., Lefebvre, E., 2008. Fast unfolding of communities in large networks. *J. Stat. Mech.: Theory Exp.* 2008, P10008.
- Braun, U., Schafer, A., Walter, H., Erk, S., Romanczuk-Seiferth, N., Haddad, L., Schweiger, J.J., Grimm, O., Heinz, A., Tost, H., Meyer-Lindenberg, A., Bassett, D.S., 2015. Dynamic reconfiguration of frontal brain networks during executive cognition in humans. *Proc. Natl. Acad. Sci. USA* 112, 11678–11683.
- Brun, C.C., Lepore, N., Pennec, X., Lee, A.D., Barysheva, M., Madsen, S.K., Avedissian, C., Chou, Y.-Y., De Zubicaray, G.I., McMahon, K.L., 2009. Mapping the regional influence of genetics on brain structure variability—a tensor-based morphometry study. *Neuroimage* 48, 37–49.
- Buckner, R.L., Krienen, F.M., 2013. The evolution of distributed association networks in the human brain. *Trends Cogn. Sci.* 17, 648–665.
- Bullmore, E., Sporns, O., 2012. The economy of brain network organization. *Nat. Rev. Neurosci.* 13, 336–349.
- Calhoun, V.D., Miller, R., Pearlson, G., Adali, T., 2014. The chronnectome: time-varying connectivity networks as the next frontier in fMRI data discovery. *Neuron* 84, 262–274.
- Casey, B., Tottenham, N., Liston, C., Durston, S., 2005. Imaging the developing brain: what have we learned about cognitive development? *Trends Cogn. Sci.* 9, 104–110.
- Chang, C., Liu, Z.M., Chen, M.C., Liu, X., Duyn, J.H., 2013. EEG correlates of time-varying BOLD functional connectivity. *NeuroImage* 72, 227–236.
- Chen, C.H., Gutierrez, E.D., Thompson, W., Panizzon, M.S., Jernigan, T.L., Eyer, L.T., Fennema-Notestine, C., Jak, A.J., Neale, M.C., Franz, C.E., Lyons, M.J., Grant, M.D., Fischl, B., Seidman, L.J., Tsuang, M.T., Kremen, W.S., Dale, A.M., 2012. Hierarchical genetic organization of human cortical surface area. *Science* 335, 1634–1636.
- Clancy, B., Darlington, R.B., Finlay, B.L., 2000. The course of human events: predicting the timing of primate neural development. *Dev. Sci.* 3, 57–66.
- Cole, M.W., Pathak, S., Schneider, W., 2010. Identifying the brain's most globally connected regions. *Neuroimage* 49, 3132–3148.
- Cole, M.W., Bassett, D.S., Power, J.D., Braver, T.S., Petersen, S.E., 2014. Intrinsic and task-evoked network architectures of the human brain. *Neuron* 83, 238–251.
- Cole, M.W., Reynolds, J.R., Power, J.D., Repovs, G., Anticicic, A., Braver, T.S., 2013. Multi-task connectivity reveals flexible hubs for adaptive task control. *Nat. Neurosci.* 16, 1348–1355.
- Craddock, R.C., James, G.A., Holtzheimer, P.E., 3rd, Hu, X.P., Mayberg, H.S., 2012. A whole brain fMRI atlas generated via spatially constrained spectral clustering. *Hum. Brain Mapp.* 33, 1914–1928.
- Crossley, N.A., Mechelli, A., Vertes, P.E., Winton-Brown, T.T., Patel, A.X., Ginestet, C.E., McGuire, P., Bullmore, E.T., 2013. Cognitive relevance of the community structure of the human brain functional coactivation network. *Proc. Natl. Acad. Sci. USA* 110, 11583–11588.
- Damaraju, E., Allen, E.A., Belger, A., Ford, J.M., McEwen, S., Mathalon, D.H., Mueller, B.A., Pearlson, G.D., Potkin, S.G., Preda, A., Turner, J.A., Vaidya, J.G., van Erp, T.G., Calhoun, V.D., 2014. Dynamic functional connectivity analysis reveals transient states of dysconnectivity in schizophrenia. *NeuroImage: Clin.* 5, 298–308.
- Deco, G., Jirsa, V.K., McIntosh, A.R., 2011. Emerging concepts for the dynamical organization of resting-state activity in the brain. *Nat. Rev. Neurosci.* 12, 43–56.
- Deco, G., Jirsa, V.K., McIntosh, A.R., 2013. Resting brains never rest: computational insights into potential cognitive architectures. *Trends Neurosci.* 36, 268–274.
- Di, X., Biswal, B.B., 2015. Dynamic brain functional connectivity modulated by resting-state networks. *Brain Struct. Funct.* 220, 37–46.
- Dubois, J., Adolphs, R., 2016. Building a science of individual differences from fMRI. *Trends Cogn. Sci.* 20, 425–443.
- Eickhoff, S.B., Stephan, K.E., Mohlberg, H., Grefkes, C., Fink, G.R., Amunts, K., Zilles, K., 2005. A new SPM toolbox for combining probabilistic cytoarchitectonic maps and functional imaging data. *Neuroimage* 25, 1325–1335.
- Finn, E.S., Shen, X., Scheinost, D., Rosenberg, M.D., Huang, J., Chun, M.M., Papademetris, X., Constable, R.T., 2015. Functional connectome fingerprinting: identifying individuals using patterns of brain connectivity. *Nat. Neurosci.* 18, 1664–1671.
- Fornito, A., Zalesky, A., Bullmore, E.T., 2010. Network scaling effects in graph analytic studies of human resting-state fMRI data. *Front. Syst. Neurosci.* 4, 22.
- Fortunato, S., 2010. Community detection in graphs. *Phys. Rep.* 486, 75–174.
- Fox, M.D., Zhang, D., Snyder, A.Z., Raichle, M.E., 2009. The global signal and observed anticorrelated resting state brain networks. *J. Neurophysiol.* 101, 3270–3283.
- Friston, K.J., Williams, S., Howard, R., Frackowiak, R.S., Turner, R., 1996. Movement-related effects in fMRI time-series. *Magn. Reson. Med.* 35, 346–355.
- Frost, M.A., Goebel, R., 2012. Measuring structural-functional correspondence: spatial variability of specialised brain regions after macro-anatomical alignment. *Neuroimage* 59, 1369–1381.
- Gao, W., Elton, A., Zhu, H., Alcauter, S., Smith, J.K., Gilmore, J.H., Lin, W., 2014. Intersubject variability of and genetic effects on the brain's functional connectivity during infancy. *J. Neurosci.* 34, 11288–11296.
- Glasser, M.F., Sotiropoulos, S.N., Wilson, J.A., Coalson, T.S., Fischl, B., Andersson, J.L., Xu, J., Jbabdi, S., Webster, M., Polimeni, J.R., Van Essen, D.C., Jenkinson, M., Consortium, W.U.-M.H., 2013. The minimal preprocessing pipelines for the human connectome project. *Neuroimage* 80, 105–124.
- Gordon, E.M., Laumann, T.O., Adeyemo, B., Petersen, S.E., 2015. Individual variability of the system-level organization of the human brain. *Cereb. Cortex.* <http://dx.doi.org/10.1093/cercor/bhv1239>.
- Gu, S., Satterthwaite, T.D., Medaglia, J.D., Yang, M., Gur, R.E., Gur, R.C., Bassett, D.S., 2015. Emergence of system roles in normative neurodevelopment. *Proc. Natl. Acad. Sci. USA* 112, 13681–13686.
- Guimera, R., Mossa, S., Turtschi, A., Amaral, L.A., 2005. The worldwide air transportation network: anomalous centrality, community structure, and cities' global roles. *Proc. Natl. Acad. Sci. USA* 102, 7794–7799.
- Haimovici, A., Tagliazucchi, E., Balenzuela, P., Chialvo, D.R., 2013. Brain organization into resting state networks emerges at criticality on a model of the human connectome. *Phys. Rev. Lett.* 110, 178101.
- Hansen, E.C., Battaglia, D., Spiegler, A., Deco, G., Jirsa, V.K., 2015. Functional connectivity dynamics: modeling the switching behavior of the resting state. *NeuroImage* 105, 525–535.
- Hartwell, L.H., Hopfield, J.J., Leibler, S., Murray, A.W., 1999. From molecular to modular cell biology. *Nature* 402, C47–C52.
- He, Y., Wang, J., Wang, L., Chen, Z.J., Yan, C., Yang, H., Tang, H., Zhu, C., Gong, Q., Zang, Y., Evans, A.C., 2009. Uncovering intrinsic modular organization of spontaneous brain activity in humans. *PLoS One* 4, e5226.
- Hill, J., Inder, T., Neil, J., Dierker, D., Harwell, J., Van Essen, D., 2010b. Similar patterns of cortical expansion during human development and evolution. *Proc. Natl. Acad. Sci. USA* 107, 13135–13140.
- Hill, J., Dierker, D., Neil, J., Inder, T., Knutsen, A., Harwell, J., Coalson, T., Van Essen, D., 2010a. A surface-based analysis of hemispheric asymmetries and folding of cerebral cortex in term-born human infants. *J. Neurosci.* 30, 2268–2276.
- Hindriks, R., Adhikari, M., Murayama, Y., Ganzetti, M., Mantini, D., Logothetis, N., Deco, G., 2015. Can sliding-window correlations reveal dynamic functional connectivity in resting-state fMRI? *Neuroimage* 127, 242–256.
- Hutchison, R.M., Morton, J.B., 2015. Tracking the brain's functional coupling dynamics over development. *J. Neurosci.* 35, 6849–6859.
- Hutchison, R.M., Womelsdorf, T., Gati, J.S., Everling, S., Menon, R.S., 2013b. Resting-state networks show dynamic functional connectivity in awake humans and anesthetized macaques. *Hum. Brain Mapp.* 34, 2154–2177.
- Hutchison, R.M., Womelsdorf, T., Allen, E.A., Bandettini, P.A., Calhoun, V.D., Corbetta, M., Penna, S., Duyn, J.H., Glover, G.H., Gonzalez-Castillo, J., Handwerker, D.A., Keilholz, S., Kiviniemi, V., Leopold, D.A., Pasquale, F., Sporns, O., Walter, M., Chang, C., 2013a. Dynamic functional connectivity: promise, issues, and interpretations. *NeuroImage* 80, 360–378.
- Johnson, M.B., Kawasawa, Y.I., Mason, C.E., Krsnik, Ž., Coppola, G., Bogdanović, D., Geschwind, D.H., Mane, S.M., State, M.W., Sestan, N., 2009. Functional and evolutionary insights into human brain development through global transcriptome analysis. *Neuron* 62, 494–509.
- Jones, D.T., Vemuri, P., Murphy, M.C., Gunter, J.L., Senjem, M.L., Machulda, M.M., Przybelski, S.A., Gregg, B.E., Kantarci, K., Knopman, D.S., Boeve, B.F., Petersen, R.C., Jack, C.R., Jr., 2012. Non-stationarity in the "resting brain's" modular architecture. *PLoS One* 7, e39731.
- Jung, R.E., Haier, R.J., 2007. The parieto-frontal integration theory (P-FIT) of intelligence: converging neuroimaging evidence. *Behav. Brain Sci.* 30, 135–187.
- Kelly, C., Biswal, B.B., Craddock, R.C., Castellanos, F.X., Milham, M.P., 2012. Characterizing variation in the functional connectome: promise and pitfalls. *Trends Cogn. Sci.* 16, 181–188.
- Kuhn, H.W., 1955. The Hungarian method for the assignment problem. *Nav. Res. Logist. Q.* 2, 83–97.
- Langs, G., Wang, D., Golland, P., Mueller, S., Pan, R., Sabuncu, M.R., Sun, W., Li, K., Liu, H., 2016. Identifying shared brain networks in individuals by decoupling functional and anatomical variability. *Cereb. Cortex* 26, 4004–4014.
- Laumann, T.O., Snyder, A.Z., Mitra, A., Gordon, E.M., Gratton, C., Adeyemo, B., Gilmore, A.W., Nelson, S.M., Berg, J.J., Greene, D.J., 2016. On the stability of BOLD fMRI correlations. *Cereb. Cortex.* <http://dx.doi.org/10.1093/cercor/bhv1265>.
- Laumann, T.O., Gordon, E.M., Adeyemo, B., Snyder, A.Z., Joo, S.J., Chen, M.Y., Gilmore, A.W., McDermott, K.B., Nelson, S.M., Dosenbach, N.U., Schlaggar, B.L., Mumford, J.A., Poldrack, R.A., Petersen, S.E., 2015. Functional system and areal organization of a highly sampled individual human brain. *Neuron* 87, 657–670.
- Leonardi, N., Van De Ville, D., 2015. On spurious and real fluctuations of dynamic functional connectivity during rest. *Neuroimage* 104, 430–436.
- Li, X., Zhu, D., Jiang, X., Jin, C., Zhang, X., Guo, L., Zhang, J., Hu, X., Li, L., Liu, T., 2014. Dynamic functional connectomics signatures for characterization and differentiation of PTSD patients. *Hum. Brain Mapp.* 35, 1761–1778.
- Liang, X., Zou, Q., He, Y., Yang, Y., 2013. Coupling of functional connectivity and regional cerebral blood flow reveals a physiological basis for network hubs of the human brain. *Proc. Natl. Acad. Sci. USA* 110, 1929–1934.
- Liang, X., Zou, Q., He, Y., Yang, Y., 2016. Topologically reorganized connectivity architecture of default-mode, executive-control, and salience networks across working memory task loads. *Cereb. Cortex* 26, 1501–1511.
- Liao, X., Yuan, L., Zhao, T., Dai, Z., Shu, N., Xia, M., Yang, Y., Evans, A., He, Y., 2015. Spontaneous functional network dynamics and associated structural substrates in the human brain. *Front. Hum. Neurosci.* 9, 478.
- Liu, X., Duyn, J.H., 2013. Time-varying functional network information extracted from

- brief instances of spontaneous brain activity. *Proc. Natl. Acad. Sci. USA* 110, 4392–4397.
- Lowe, M., Mock, B., Sorenson, J., 1998. Functional connectivity in single and multislice echoplanar imaging using resting-state fluctuations. *Neuroimage* 7, 119–132.
- Meunier, D., Lambiotte, R., Bullmore, E.T., 2010. Modular and hierarchically modular organization of brain networks. *Front. Neurosci.* 4, 200.
- Meunier, D., Achard, S., Morcom, A., Bullmore, E., 2009. Age-related changes in modular organization of human brain functional networks. *Neuroimage* 44, 715–723.
- Moussa, M.N., Steen, M.R., Laurienti, P.J., Hayasaka, S., 2012. Consistency of network modules in resting-state fMRI connectome data. *PLoS One* 7, e44428.
- Mueller, S., Wang, D., Fox, M.D., Yeo, B.T., Sepulcre, J., Sabuncu, M.R., Shafiq, R., Lu, J., Liu, H., 2013. Individual variability in functional connectivity architecture of the human brain. *Neuron* 77, 586–595.
- Murphy, K., Birn, R.M., Handwerker, D.A., Jones, T.B., Bandettini, P.A., 2009. The impact of global signal regression on resting state correlations: are anti-correlated networks introduced? *NeuroImage* 44, 893–905.
- Newman, M.E., 2004. Fast algorithm for detecting community structure in networks. *Phys. Rev. E* 69, 066133.
- Newman, M.E., 2006. Modularity and community structure in networks. *Proc. Natl. Acad. Sci. USA* 103, 8577–8582.
- Pessoa, L., 2014. Understanding brain networks and brain organization. *Phys. Life Rev.* 11, 400–435.
- Petanjek, Z., Judas, M., Simic, G., Rasin, M.R., Uylings, H.B., Rakic, P., Kostovic, I., 2011. Extraordinary neoteny of synaptic spines in the human prefrontal cortex. *Proc. Natl. Acad. Sci. USA* 108, 13281–13286.
- Pinel, P., Thirion, B., Meriaux, S., Jobert, A., Serres, J., Le Bihan, D., Poline, J.B., Dehaene, S., 2007. Fast reproducible identification and large-scale databasing of individual functional cognitive networks. *Neuron* 79, 798–813.
- Power, J.D., 2016. A simple but useful way to assess fMRI scan qualities. *NeuroImage*. <http://dx.doi.org/10.1016/j.neuroimage.2016.1008.1009>.
- Power, J.D., Schlaggar, B.L., Petersen, S.E., 2015. Recent progress and outstanding issues in motion correction in resting state fMRI. *Neuroimage* 105, 536–551.
- Power, J.D., Schlaggar, B.L., Lessov-Schlaggar, C.N., Petersen, S.E., 2013. Evidence for hubs in human functional brain networks. *Neuron* 79, 798–813.
- Power, J.D., Cohen, A.L., Nelson, S.M., Wig, G.S., Barnes, K.A., Church, J.A., Vogel, A.C., Laumann, T.O., Miezin, F.M., Schlaggar, B.L., Petersen, S.E., 2011. Functional network organization of the human brain. *Neuron* 72, 665–678.
- Prichard, D., Theiler, J., 1994. Generating surrogate data for time series with several simultaneously measured variables. *Phys. Rev. Lett.* 73, 951–954.
- Richiardi, J., Altmann, A., Milazzo, A.C., Chang, C., Chakravarty, M.M., Banaschewski, T., Barker, G.J., Bokde, A.L., Bromberg, U., Buchel, C., Conrod, P., Fauth-Bühler, M., Flor, H., Frouin, V., Gallinat, J., Garavan, H., Gowland, P., Heinz, A., Lemaitre, H., Mann, K.F., Martinot, J.L., Nees, F., Paus, T., Pausova, Z., Rietschel, M., Robbins, T.W., Smolka, M.N., Spanagel, R., Strohle, A., Schumann, G., Hawrylycz, M., Poline, J.B., Greicius, M.D., consortium, I., 2015. Correlated gene expression supports synchronous activity in brain networks. *Science* 348, 1241–1244.
- Rosvall, M., Bergstrom, C.T., 2008. Maps of random walks on complex networks reveal community structure. *Proc. Natl. Acad. Sci. USA* 105, 1118–1123.
- Sadaghiani, S., Poline, J.B., Kleinschmidt, A., D'Esposito, M., 2015. Ongoing dynamics in large-scale functional connectivity predict perception. *Proc. Natl. Acad. Sci. USA* 112, 8463–8468.
- Schaefer, A., Margulies, D.S., Lohmann, G., Gorgolewski, K.J., Smallwood, J., Kiebel, S.J., Villringer, A., 2014. Dynamic network participation of functional connectivity hubs assessed by resting-state fMRI. *Front. Hum. Neurosci.* 8, 195.
- Schultz, D.H., Cole, M.W., 2016. Higher intelligence is associated with less task-related brain network reconfiguration. *J. Neurosci.* 36, 8551–8561.
- Shen, X., Tokoglu, F., Papademetris, X., Constable, R.T., 2013. Groupwise whole-brain parcellation from resting-state fMRI data for network node identification. *Neuroimage* 82, 403–415.
- Smith, S.M., Fox, P.T., Miller, K.L., Glahn, D.C., Fox, P.M., Mackay, C.E., Filippini, N., Watkins, K.E., Toro, R., Laird, A.R., Beckmann, C.F., 2009. Correspondence of the brain's functional architecture during activation and rest. *Proc. Natl. Acad. Sci. USA* 106, 13040–13045.
- Sporns, O., Betzel, R.F., 2016. Modular brain networks. *Annu. Rev. Psychol.* 67, 613–640.
- Steen, M., Hayasaka, S., Joyce, K., Laurienti, P., 2011. Assessing the consistency of community structure in complex networks. *Phys. Rev. E* 84, 016111.
- Tagliazucchi, E., Balenzuela, P., Fraiman, D., Chialvo, D.R., 2012a. Criticality in large-scale brain fMRI dynamics unveiled by a novel point process analysis. *Front. Physiol.* 3, 15.
- Tagliazucchi, E., Von Wegner, F., Morzelewski, A., Brodbeck, V., Laufs, H., 2012b. Dynamic BOLD functional connectivity in humans and its electrophysiological correlates. *Front. Hum. Neurosci.* 6, 339.
- Van Essen, D.C., Dierker, D.L., 2007. Surface-based and probabilistic atlases of primate cerebral cortex. *Neuron* 56, 209–225.
- Van Essen, D.C., Smith, S.M., Barch, D.M., Behrens, T.E., Yacoub, E., Ugurbil, K., Consortium, W.U.-M.H., 2013. The WU-minn human connectome project: an overview. *Neuroimage* 80, 62–79.
- Vinh, N.X., Epps, J., Bailey, J., 2010. Information theoretic measures for clusterings comparison: variants, properties, normalization and correction for chance. *J. Mach. Learn. Res.* 11, 2837–2854.
- Wang, C., Ong, J.L., Patanaik, A., Zhou, J., 2016. Spontaneous eyelid closures link vigilance fluctuation with fMRI dynamic connectivity states. *Proc. Natl. Acad. Sci. USA* 113, 9653–9658.
- Wang, D., Buckner, R.L., Fox, M.D., Holt, D.J., Holmes, A.J., Stoecklein, S., Langs, G., Pan, R., Qian, T., Li, K., Baker, J.T., Stufflebeam, S.M., Wang, K., Wang, X., Hong, B., Liu, H., 2015a. Parcellating cortical functional networks in individuals. *Nat. Neurosci.* 18, 1853–1860.
- Wang, J., Wang, X., Xia, M., Liao, X., Evans, A., He, Y., 2015b. GRETA: a graph theoretical network analysis toolbox for imaging connectomics. *Front. Hum. Neurosci.* 9, 386.
- Wang, J., Wang, L., Zang, Y., Yang, H., Tang, H., Gong, Q., Chen, Z., Zhu, C., He, Y., 2009. Parcellation-dependent small-world brain functional networks: a resting-state fMRI study. *Hum. Brain Mapp.* 30, 1511–1523.
- Weissenbacher, A., Kasess, C., Gerstl, F., Lanzenberger, R., Moser, E., Windischberger, C., 2009. Correlations and anticorrelations in resting-state functional connectivity MRI: a quantitative comparison of preprocessing strategies. *NeuroImage* 47, 1408–1416.
- Wig, G.S., Schlaggar, B.L., Petersen, S.E., 2011. Concepts and principles in the analysis of brain networks. *Ann. N. Y. Acad. Sci.* 1224, 126–146.
- Xia, M., Wang, J., He, Y., 2013. BrainNet Viewer: a network visualization tool for human brain connectomics. *PLoS One* 8, e68910.
- Yan, C., Zang, Y., 2010. DPARSF: a MATLAB toolbox for "pipeline" data analysis of resting-state fMRI. *Front. Syst. Neurosci.* 4, 13.
- Yan, C.G., Cheung, B., Kelly, C., Colcombe, S., Craddock, R.C., Di Martino, A., Li, Q., Zuo, X.N., Castellanos, F.X., Milham, M.P., 2013. A comprehensive assessment of regional variation in the impact of head micromovements on functional connectomics. *Neuroimage* 76, 183–201.
- Yeo, B.T.T., Krienen, F.M., Eickhoff, S.B., Yaakub, S.N., Fox, P.T., Buckner, R.L., Asplund, C.L., Chee, M.W.L., 2015. Functional specialization and flexibility in human association cortex. *Cereb. Cortex* 25, 3654–3672.
- Zalesky, A., Breakspear, M., 2015. Towards a statistical test for functional connectivity dynamics. *Neuroimage* 114, 466–470.
- Zalesky, A., Fornito, A., Cocchi, L., Gollo, L.L., Breakspear, M., 2014. Time-resolved resting-state brain networks. *Proc. Natl. Acad. Sci. USA* 111, 10341–10346.
- Zeng, L.L., Wang, D., Fox, M.D., Sabuncu, M., Hu, D., Ge, M., Buckner, R.L., Liu, H., 2014. Neurobiological basis of head motion in brain imaging. *Proc. Natl. Acad. Sci. USA* 111, 6058–6062.
- Zhang, J., Cheng, W., Liu, Z., Zhang, K., Lei, X., Yao, Y., Becker, B., Liu, Y., Kendrick, K.M., Lu, G., Feng, J., 2016. Neural, electrophysiological and anatomical basis of brain-network variability and its characteristic changes in mental disorders. *Brain* 139, 2307–2321.
- Zilles, K., Amunts, K., 2013. Individual variability is not noise. *Trends Cogn. Sci.* 17, 153–155.